

THE X-RAY STRUCTURE OF THE PULSAR BOW SHOCK G189.22+2.90 IN THE SUPERNOVA REMNANT IC 443

B. M. GAENSLER,^{1,2,3} S. CHATTERJEE,^{4,1} P. O. SLANE,¹ E. VAN DER SWALUW,⁵ F. CAMILO⁶ AND J. P. HUGHES⁷

To appear in The Astrophysical Journal

ABSTRACT

We present a deep observation with the *Chandra X-ray Observatory* of the neutron star bow shock G189.22+2.90 in the supernova remnant (SNR) IC 443. Our data confirm the cometary morphology and central point source seen previously, but also reveal considerable new structure. Specifically, we find that the X-ray nebula consists of two distinct components: a “tongue” of bright emission close to the neutron star, enveloped by a larger, fainter “tail”. We interpret the tongue and tail as delineating the termination shock and the post-shock flow, respectively, as previously identified also in the pulsar bow shock G359.23–0.82 (“the Mouse”). However, for G189.22+2.90 the tongue is much less elongated than for the Mouse, while the tail is much broader. These differences are consistent with the low Mach number, $\mathcal{M} \lesssim 2$, expected for a neutron star moving through the hot gas in a SNR’s interior, supporting the case for a physical association between G189.22+2.90 and IC 443. We resolve the stand-off distance between the star and the head of the bow shock, which allows us to estimate a space velocity for the neutron star of $\sim 230 \text{ km s}^{-1}$, independent of distance. We detect thermal emission from the neutron star surface at a temperature of $102 \pm 22 \text{ eV}$, which is consistent with the age of SNR IC 443 for standard neutron star cooling models. We also identify two compact knots of hard emission located $1'' - 2''$ north and south of the neutron star.

Subject headings: ISM: individual: (G189.22+2.90, IC 443) — pulsars: individual (CXOU J061705.3+222127) — stars: neutron — stars: winds, outflows

1. INTRODUCTION

The relativistic winds from energetic pulsars generate broadband synchrotron emission when they interact with their surroundings. New high resolution X-ray observations have revealed amazing details in the structure of the resulting pulsar wind nebulae (PWNe) (Weisskopf & Hughes 2006; Gaensler & Slane 2006). Most of these systems resemble the Crab Nebula, and typify early phases of PWN evolution. However, after a few thousand years a pulsar’s motion becomes supersonic with respect to its surroundings, and a bow shock is formed. While only a small group of pulsar bow shocks have been as yet identified, these sources provide an additional opportunity to probe pulsar winds, using very different boundary conditions from those experienced by “Crab-like” PWNe.

Gaensler et al. (2004), hereafter G2004, presented a detailed study of G359.23–0.82 (“the Mouse”), a spectacular radio and X-ray bow shock powered by the energetic pulsar J1747–2958. This analysis led to the identification of distinctive features which should also be observable in other bow shocks. A comparable system is G189.22+2.90 (also known as 1SAX J0617.1+2221), an apparent X-ray and radio bow shock coincident with the supernova remnant (SNR) IC 443, as shown in Figure 1 (see also Olbert et al. 2001, hereafter O2001; Bocchino & Bykov 2001). Pulsations from

a pulsar in G189.22+2.90 have not yet been detected, but the nebula’s cometary morphology, with a point source near the apex, make it virtually certain that this is a pulsar-driven bow shock. Here we present a deep *Chandra* observation of G189.22+2.90, with which we study the structure of this source and compare it to that seen for the Mouse.

Before discussing this system further, we note that it is unclear if G189.22+2.90 and IC 443 are genuinely associated because, as can be seen in Figure 1, the cometary trail of G189.22+2.90 points $\sim 80^\circ$ away from the direction expected if the embedded pulsar is moving away from the SNR’s center. Despite this difficulty, for now we assume that the pulsar, PWN and SNR are physically associated, and consequently adopt a common distance to them of $1.5d_{1.5} \text{ kpc}$ (Welsh & Sallmen 2003). In §4.4 we will discuss the validity of this assumption in the light of the new data presented here.

2. OBSERVATIONS AND ANALYSIS

The earlier observations of O2001 were carried out using the ACIS-I3 CCD of *Chandra* on 2000 April 10–11 (ObsID 760), with G189.22+2.90 located $3'$ off-axis. Our more recent observations were performed using the ACIS-S3 CCD on 2005 January 12–13 (ObsID 5531), with the source positioned close to the aimpoint. We have analyzed both datasets using CIAO v3.3 and CALDB v3.2.1. For the data from 2000, we applied a known aspect offset to the data-set, and then reprocessed the event list⁸ to identify hot pixels and afterglows. For both data-sets, the latest ACIS gain map, the time-dependent gain correction, and a correction for charge transfer inefficiency were all applied. The data were then filtered for bad event grades, good time intervals and flaring. The final usable exposures were 9.6 ks and 37.5 ks for the 2000 and 2005 data, respectively.

An image from the 2005 data in the energy range 0.3–10 keV is shown in Figure 2(a). A smoothed version, with ra-

¹ Harvard-Smithsonian Center for Astrophysics, 60 Garden Street, Cambridge, MA 02138; bgaensler@cfa.harvard.edu

² Alfred P. Sloan Research Fellow

³ Present address: School of Physics A29, University of Sydney, NSW 2006, Australia

⁴ Jansky Fellow, National Radio Astronomy Observatory, 520 Edgemont Road, Charlottesville, VA 22903

⁵ Royal Netherlands Meteorological Institute (KNMI), PO Box 201, 3730 AE De Bilt, The Netherlands

⁶ Columbia Astrophysics Laboratory, Columbia University, 550 West 120th Street, New York, NY 10027

⁷ Department of Physics and Astronomy, Rutgers University, 136 Frelinghuysen Road, Piscataway, NJ 08854

⁸ This correction was part of the standard pipeline for the 2005 data.

dio contours from O2001 overlaid, is presented in Figure 2(b). The resulting image is ~ 6 times deeper than that from the 2000 data of O2001.

For spectroscopy, we combined the two data-sets. We used identical source extraction regions for each observation (see Fig. 2[b]), and then created corresponding weighted response and effective area files using the CIAO script `specextract`. Spectra were grouped so that there was a minimum of 25 counts per channel (with the exception of the 2000-epoch spectrum of the central source CXOU J061705.3+222127 [see §3.1], which was grouped to 15 counts per channel because of the low number of counts). For background spectra, we used annular regions immediately surrounding each of the regions shown in Figure 2(b). Spectra were then modeled using XSPEC v11.3.1. In all spectral fitting, we jointly fit the two observations from 2000 and 2005, with all model parameters locked between the two data-sets.

3. RESULTS

3.1. Images

We identify a number of notable features from the X-ray and radio images shown in Figure 2:

1. As earlier identified by O2001, there is a bright compact source near the apex of the nebula, which they designated CXOU J061705.3+222127 (hereafter J0617+2221). A gaussian fit to this source yields a position RA (J2000) $06^{\text{h}}17^{\text{m}}05^{\text{s}}.18 \pm 0^{\text{s}}.02$, Decl. (J2000) $+22^{\circ}21'27''.6 \pm 0''.3$, where the dominant source of error is the precision to which we can register the nearby infrared source 2MASS 06171300+2220587 to its X-ray counterpart.
2. The image in Figure 2(a) strongly suggests that there is extended structure $1'' - 2''$ to the north and south of J0617+2221. We have investigated this by fitting a gaussian with the dimensions of the point spread function to the emission at the position of J0617+2221, and then subtracting this from the data. With the unresolved component (~ 200 counts) removed, the inset to Figure 2(a) demonstrates the clear presence of two compact components of emission to the north and south of J0617+2221, each containing $\sim 30 - 40$ counts.
3. On larger scales, an elongated diffuse region with a “bullet” morphology is seen, which following from our earlier studies of the Mouse (G2004), we designate “the tongue”. Defining the tongue’s perimeter to be the locus at which the emission falls to 10% of the peak in Figure 2(b), we find that the tongue is oriented at a position angle of $+50^{\circ}$ (N through E), and has an approximate extent of $33'' \times 15''$. Along its major axis, the tongue extends $8'' \pm 1''$ ahead of J0617+2221, and $25'' \pm 1''$ behind it. The tongue is also a feature of enhanced brightness at radio wavelengths (contours in Fig. 2[b]).
4. Surrounding the tongue, we identify a larger diffuse X-ray region, best seen in Figure 2(b), which we designate “the tail”. The tail has a cometary shape, but with a broader opening angle than the tongue. It is sharply bounded at its apex, but fades into the background toward the rear. The tail is the brightest part of a larger X-ray structure seen by *XMM-Newton* (Bocchino & Bykov 2001).

3.2. Spectroscopy

We have extracted spectra for the three regions shown in Figure 2(b), corresponding to J0617+2221, the tongue, and the tail.

To accurately estimate the foreground absorbing column, N_H , we fit simultaneous absorbed power laws to the large number of counts obtained for the tongue and the tail, constrained to have the same N_H , but with independent photon indices. The results are given in Table 1, showing that both regions are good fits to power law spectra, with a foreground column $N_H = (7.2 \pm 0.6) \times 10^{21} \text{ cm}^{-2}$ (this and all subsequent errors are at 90% confidence). The photon indices for the two regions are the same within the errors.

We then fit to the spectrum of J0617+2221, excluding most of the emission from the compact structures immediately surrounding it by using a circular extraction region of radius $1''.4$. If we constrain N_H to lie in the range inferred above, we find that both a power law and a blackbody are poor fits to the data, both models not accounting for a hard excess seen above 2 keV. A combined fit of a blackbody and a power law resolves this problem and produces an excellent fit, as listed in Table 1 and shown in Figure 3.

We have also tried to fit spectra to the compact knots seen on either side of the pulsar. However, since each knot only contains ~ 40 counts in the combined data-set, we are unable to derive useful spectral parameters for these regions. Simple hardness ratios indicate that both these knots are significantly harder than J0617+2221, suggesting that their emission is probably non-thermal.

4. DISCUSSION

Our new data clearly confirm the main result of O2001: G189.22+2.90 consists of a compact source at the apex of a striking cometary nebula, which presumably represent an energetic pulsar and its wind-driven bow shock, respectively. Here we focus on the additional information provided by the higher sensitivity and improved angular resolution of our new data.

4.1. The Neutron Star

We first consider the X-ray emission from J0617+2221. O2001 assumed that the X-rays from J0617+2221 were thermal. They adopted a low absorbing column $N_H = 1.3 \times 10^{21} \text{ cm}^{-2}$, and consequently found a very high temperature (≈ 0.7 keV) and a small emitting area ($\approx 0.025 d_{1.5}^2 \text{ km}^2$). With better statistics but limited spatial resolution, Bocchino & Bykov (2001) were unable to directly detect X-rays from J0617+2221, but found that a blackbody with a temperature 0.13 keV and radius 3.3 km was consistent with their data.

Here we directly detect thermal emission from J0617+2221, confirming its identification as a neutron star. The blackbody component of the fit to J0617+2221 shown in Figure 3 implies an emitting radius (as viewed at infinity) of $6_{-3}^{+8} d_{1.5} \text{ km}$. This is not especially constraining, being consistent both with cooling emission from the whole surface, and also with the smaller radii seen for blackbody fits to neutron star atmospheres (e.g., Pavlov et al. 2001; McGowan et al. 2004). The inferred temperature and bolometric luminosity, as viewed at infinity, are $kT^{\infty} = 102 \pm 22 \text{ eV}$ and $L^{\infty} = 5.0_{-2.2}^{+5.0} d_{1.5}^2 \times 10^{32} \text{ ergs s}^{-1}$, respectively. The age estimated for IC 443 is ~ 30000 years (Chevalier 1999). Assuming that J0617+2221 is associated

with IC 443, has a mass in the range 1.35-1.45 M_{\odot} and has a 1p proton superfluid core, the neutron star's predicted surface temperature is $kT^{\infty} = 60 - 110$ eV, and its expected luminosity is $L^{\infty} = 10^{32} - 10^{34}$ ergs s^{-1} (e.g., Kaminker et al. 2002; Page et al. 2006). Thus, while we are not able to distinguish between different neutron star cooling models, the thermal emission from J0617+2221 is consistent with "standard" cooling at the age estimated for IC 443.

As discussed in §3.2, the X-ray spectrum of J0617+2221 also requires a significant non-thermal component. We interpret this as magnetospheric emission from the pulsar, which typically has a photon index $\Gamma \sim 2$ (e.g., Pavlov et al. 2001; Mineo et al. 2002; Jackson & Halpern 2005), consistent with the fit obtained here. In this case, we expect these X-rays to be strongly pulsed, as is seen for several other young and energetic pulsars (see Kaspi et al. 2006, for a review). This possibility can be tested through a future observation with the *Chandra* High Resolution Camera.

4.2. Compact Structures Close to the Neutron Star

We will argue in §4.3.1 that the tongue region in which J0617+2221 is embedded traces the outer surface of the wind termination shock. Since the region interior to this corresponds to cold, unshocked wind material which should not emit, the compact X-ray structures seen close to the neutron star likely lie outside the tongue, but projected against it.

As two emitting components on either side of the pulsar, there is the temptation to identify these structures as polar jets, as have been seen for several Crab-like PWNe (e.g., Weisskopf et al. 2000; Helfand et al. 2001). Such jets are now understood to be formed beyond the wind termination shock by equatorially outflowing particles which reverse in flow direction and which are then collimated along the spin axis via hoop stress (Komissarov & Lyubarsky 2003; Del Zanna et al. 2004). For the Crab Nebula, the reversal of the equatorial flow depends on the confining thermal pressure into which the PWN expands (Komissarov & Lyubarsky 2003). However, for G189.22+2.90, ram pressure produces a very different set of boundary conditions, for which it is as yet unclear if such structures can form. Alternatively, X-ray knots close to the pulsar have been seen in PWNe such as the Crab Nebula, G320.4-1.2, G292.0+1.8 and the Mouse (Hester et al. 2002; Gaensler et al. 2002a; Hughes et al. 2003, G2004). Komissarov & Lyubarsky (2004) propose that these features are relativistically beamed components beyond the termination shock, where the shocked flow travels along a curved surface.

In either interpretation, such structures should define the projected spin axis of the neutron star, as has been argued for the Crab pulsar and several other sources (Ng & Romani 2004). If the projected velocity vector of J0617+2221 is defined by the bow-shock morphology, then G189.22+2.90 would represent an example of substantial misalignment between the pulsar's spin axis and its velocity vector. This would be in sharp contrast to other systems for which "spin-kick alignment" has been claimed, and would have important implications for the formation mechanism of neutron stars (Lai et al. 2001). Alternatively, as discussed below in §4.4, the pulsar may in fact be moving to the south, away from the center of SNR IC 443. In this case the spin and velocity vectors would show approximate alignment, and the bow-shock morphology would trace the effect of surrounding bulk flows rather than of the pulsar's motion. We are developing full three-dimensional hydrodynamic models of bow

shocks with anisotropic outflows to address these possibilities (Vigelius et al. 2006).

4.3. The Nebula

Cometary X-ray nebulae behind moving neutron stars have now been seen by *Chandra* and *XMM-Newton* for several sources (Gaensler & Slane 2006, and references therein). However, what our new data make clear is that G189.22+2.90 is clearly structured into two distinct components: the bright tongue, and the fainter surrounding tail. We previously identified this same spatial decomposition for the Mouse, and adopt a similar interpretation here: namely that the bullet-shaped tongue region represents the surface of the wind termination shock, while the tail corresponds to shocked material flowing downstream (see G2004 for detailed arguments and discussion).

4.3.1. The Termination Shock

We directly resolve the separation between J0617+2221 and the apex of the tongue, and so can infer a forward termination shock radius $r_{TS}^F \approx 0.06d_{1.5}$ pc. There is also a clear termination of the tongue behind J0617+2221, so we also infer a backward termination shock radius $r_{TS}^B \approx 0.2\mu d_{1.5}$ pc, where $\mu \leq 1$ is a factor which accounts for smearing of the backward termination shock as a result of ions in the wind (see §4.5 of G2004).

The ratio r_{TS}^B/r_{TS}^F is a direct diagnostic of the Mach number, \mathcal{M} , of the system. For low Mach numbers, we expect $r_{TS}^B/r_{TS}^F = \gamma^{1/2} \mathcal{M}$, where $\gamma = 5/3$ is the adiabatic coefficient of ambient gas (Bucciantini 2002; van der Swaluw et al. 2003). Here we find $r_{TS}^B/r_{TS}^F \approx 3\mu$ independent of distance, from which we infer⁹ $\mathcal{M} \approx 1.2$ for $\mu = 0.5$ (see G2004). This bow shock is only mildly supersonic, in sharp contrast to the Mouse for which we found $r_{TS}^B/r_{TS}^F \approx 13\mu$ and $\mathcal{M} \approx 60$. This is consistent with the expected conditions: the Mouse is moving through the interstellar medium (ISM) where the sound speed is low, while if G189.22+2.90 is in the SNR interior where the sound speed of hot shocked gas is high, we expect $\mathcal{M} < 3$ (see Fig. 4 of van der Swaluw et al. 2004).

If G189.22+2.90 and IC 443 are associated, we can combine the observed properties of these objects to estimate the space velocity and spin-down luminosity of J0617+2221. Kawasaki et al. (2002) find that in the outer parts of IC 443, the shocked gas has a temperature 0.2 keV, corresponding to a sound speed $c_s \approx 180$ km s^{-1} . Since J0617+2221 is near the edge of the shell of IC 443 (see Fig. 1), we adopt that value here. The pulsar velocity relative to surrounding gas is then $V_{rel} = \mathcal{M}c_s \approx 420\mu$ km s^{-1} . To determine the pulsar space velocity, we must add vectorially the local flow velocity, V_{flow} , to V_{rel} . The PWN is close to the SNR's rim, so we assume $V_{flow} \sim V_{SNR} \approx 100$ km s^{-1} (Chevalier 1999), where V_{SNR} is the velocity of the forward shock. If the local flow is directed radially outward from the SNR's geometric center, then V_{rel} and V_{flow} are approximately perpendicular. If we adopt $\mu = 0.5$, we then find a pulsar velocity $V_{PSR} \approx 230$ km s^{-1} . By assuming that the pulsar was born at the SNR's geometric center (see discussion of this point in §4.4), O2001 were able to derive an independent velocity estimate $V_{PSR} \approx 250 \pm 50$ km s^{-1} , which is in good agreement with our calculation.

We can estimate the pulsar's spin-down luminosity, \dot{E} , as follows. If G189.22+2.90 is inside the SNR but close to its

⁹ Note that the PWN's opening angle cannot be used to infer \mathcal{M} , as that only applies to the unseen forward shock.

edge, the ambient pressure is $P_0 \approx P_{sh} = 3/4 \rho_0 V_{SNR}^2$, where P_{sh} is the pressure behind the SNR's forward shock and ρ_0 is the density of the ambient ISM. Chevalier (1999) gives $\rho_0 \approx 2.5 d_{1.5}^{-1} \times 10^{-23} \text{ g cm}^{-3}$, so we infer¹⁰ $P_0 \approx 2 d_{1.5}^{-1} \times 10^{-9} \text{ ergs cm}^{-3}$. Pressure balance between the bow shock and its surroundings then implies $\dot{E}/4\pi r_{TS}^2 c = \gamma \mathcal{M}^2 P_0$ (G2004). For $\mu = 0.5$ and $d_{1.5} = 1$, we find $\dot{E} \approx 5 \times 10^{37} \text{ ergs s}^{-1}$, which would make J0617+2221 the most energetic member of the 10–100 kyr old group of “Vela-like” pulsars (see Table 5 of Kramer et al. 2003). We note that our estimate of \dot{E} is more than an order of magnitude larger than that found by assuming that the X-ray or radio luminosity of G189.22+2.90 is a fixed fraction of \dot{E} (O2001; Bocchino & Bykov 2001), illustrating the large uncertainties in all these indirect estimates of \dot{E} .

4.3.2. The Post-Shock Flow

Another difference between the Mouse and G189.22+2.90 is the morphology of the tail. For the Mouse the tail has a narrow component seen in both radio and X-rays, enveloped by a broader region seen at radio wavelengths. G2004 interpreted this as material shocked at the backward and forward termination shocks, respectively. For the latter, the flow speed is ~ 4 times higher, but the magnetic field is stronger. The resultant synchrotron losses explain its lack of X-ray emission.

In contrast to the Mouse, here the tail is composed of a single broad structure, with good correspondence between radio and X-rays. This difference can be understood as follows. Conservation of energy leads us to expect that $B_n^F/B_n^B = r_{TS}^B/r_{TS}^F$ (see Eqn. [13] of G2004), where B_n^F and B_n^B are the nebular magnetic field strengths in the flow from the forward and backward termination shocks, respectively. In this case we find $B_n^F/B_n^B \approx 3\mu$, a ratio ~ 4 times smaller than that seen in the Mouse. Factoring in the difference in flow speed between the forward and backward flow regions (Bucciantini et al. 2005), the synchrotron loss times for the two zones now become comparable. We thus expect a single combined region emitting in both the X-ray and radio bands, as observed. The power laws of the tongue and tail regions have similar photon indices (see Table 1), indicating that radiative losses are minimal over the ~ 0.5 pc scale imaged by *Chandra*. At distances $\gtrsim 2$ pc downstream, the X-ray spectrum begins to soften due to synchrotron losses, as seen by *XMM-Newton* (Bocchino & Bykov 2001).

4.4. The Association Between G189.22+2.90 and IC 443

As mentioned in §1, there are difficulties with the claimed association between G189.22+2.90 and IC 443. Most notable is the fact that the nebular symmetry axis is completely misaligned with respect to the vector running from the SNR's center to J0617+2221 (see Fig. 1). Furthermore, the failure to detect a period and period derivative for J0617+2221 prevents us from estimating the pulsar's age and comparing it to that of the SNR, while the wide range in N_H seen toward different parts of IC 443 in previous X-ray studies¹¹ makes it difficult to determine whether the PWN and SNR are at similar distances.

However, the results presented here provide new evidence in favor of a physical association. First, the surface temper-

ature measured for J0617+2221 is consistent with the age of 30 000 years inferred for the SNR. Second, as discussed in §4.3, the differences in morphology between G189.22+2.90 and the Mouse imply that either the confining media or the pulsars have very different properties. Specifically, if we repeat the estimates made in §4.3.1, but now for a pulsar not embedded inside a SNR but rather moving through a typical warm region of the ISM ($c_s \sim 10 \text{ km s}^{-1}$; $P_0 \sim 3 \times 10^{-13} \text{ ergs cm}^{-3}$), we find $V_{PSR} \approx 20 \text{ km s}^{-1}$ and $\dot{E} \approx 10^{34} d_{1.5}^2 \text{ ergs s}^{-1}$. The former is slower than 98% of the young pulsar population (Hobbs et al. 2005), while the latter would imply a $\sim 10\%$ efficiency of conversion of spin-down luminosity into the total X-ray luminosity of the system, which is higher than observed for any other pulsar and its PWN (cf., Chevalier 2000, G2004). The properties of the PWN thus argue that the pulsar wind is most likely confined by hot gas in the SNR interior.

Given these arguments for a genuine association, we then need to explain the misaligned nebular symmetry axis. A possible explanation is that the explosion site did not coincide with the SNR's geometric center. This can result if the progenitor star had a high space velocity, so that the supernova exploded at an offset position within a wind-blown cavity (Gvaramadze 2002). The pulsar's velocity vector is then directed away from the explosion site, rather than from the SNR center. Note that the offset between the explosion site and the SNR's center is probably not as extreme as suggested by the observed morphology, since gas flows in the SNR interior are likely to be skewing the orientation of G189.22+2.90.¹² This can be tested by future observations: combining the estimates of V_{rel} and V_{flow} made in §4.3 above, we expect a proper motion for J0617+2221 of $\sim 35 d_{1.5}^{-1} \text{ mas yr}^{-1}$ at a position angle of $\sim 200^\circ$, north through east. This may be measurable 5–10 years hence.

5. CONCLUSIONS

Our new *Chandra* observations of G189.22+2.90 reveal a thermally-emitting neutron star with a typical space velocity of $\sim 230 \text{ km s}^{-1}$, whose relativistic wind drives a bow shock through the shocked gas inside its associated SNR IC 443. We place this system midway between PSR B1853+01 / SNR W44 (for which the pulsar bow shock is deep in the interior of the SNR) and PSR B1951+32 / SNR CTB 80 (for which the pulsar is now crossing the SNR shell) in the evolutionary sequence described by van der Swaluw et al. (2004). While pulsations from the central source in G189.22+2.90 have not been detected in the radio band, pulsed magnetospheric emission may be detectable in future deep X-ray observations.

G189.22+2.90 shows a close correspondence with the Mouse, in that the X-ray emission from both sources consists of two distinct components, a “tongue” and a “tail”. The specific differences between these features in G189.22+2.90 and in the Mouse can be understood in terms of the much lower Mach number of the pulsar for G189.22+2.90. The presence of these features in two systems, and our ability to interpret them consistently in terms of the expected wind shock structures, argue that these are ubiquitous features in pulsar bow shocks. Deeper observations of other pulsar bow shocks (especially those with detected pulsars and known

¹⁰ A similar estimate comes from the X-ray spectrum of IC 443, which give $P_0 \approx 1 d_{1.5}^{-1/2} \times 10^{-9} \text{ ergs cm}^{-3}$ (Kawasaki et al. 2002).

¹¹ This presumably results from spatial variations in the absorption due to the well-known interaction of this SNR with a molecular cloud; see e.g., Burton et al. (1988).

¹² Gaensler et al. (2002b) proposed a similar explanation to account for the misalignment between the proper motion direction of PSR J2124–3358 and the symmetry axis of its surrounding bow shock.

TABLE 1
SPECTRAL FITS TO REGIONS OF G189.22+2.90.

Region	Total Counts ^a (0.5–10.0 keV)	N_H (10^{21} cm ⁻²)	Γ	kT^∞ (eV)	f_x (10^{-13} ergs cm ⁻² s ⁻¹) ^b	χ^2/ν
Tongue (PL)	4432 ± 96	7.2 ± 0.6 ^c	1.70 ^{+0.10} _{-0.05}	—	17 ± 1	447/511 = 0.88
Tail (PL)	6999 ± 119	''	1.73 ± 0.08	—	27 ± 2	''
Central source (PL)	313 ± 20	6.6–7.8 (constrained)	5.6 ^{+0.7} _{-0.6}	—	0.47 ^{+0.32} _{-0.09}	25/14 = 1.79
Central source (BB)	''	''	—	150 ± 20	0.21 ^{+0.15} _{-0.10}	46/14 = 3.31
Central source (BB+PL)	''	''	2.6 ^{+0.5} _{-1.0}	102 ± 22	0.45 ^{+0.46} _{-0.22}	10/12 = 0.85

NOTE. — Uncertainties are all at 90% confidence. “PL” = power law and “BB” = blackbody.

^aThe number of counts is that for the 2000 and 2005 observations combined. In each case, the 2005 data contribute ~85%–90% of the total.

^bFluxes are for the energy range 0.5–10.0 keV, and have been corrected for absorption.

^cThe spectral fits for the tongue and tail regions were constrained to have the same value of N_H .

proper motions, see Gaensler et al. 2002b; Stappers et al. 2003; Caraveo et al. 2003), in hand with new relativistic magnetohydrodynamic simulations of these systems (e.g., Bucciantini et al. 2005), can further add to our understanding of these systems.

We thank Denis Leahy for providing a radio image of IC 443, and an anonymous referee for comments which improved this paper. The Second Palomar Observatory Sky Survey (POSS-II) was made by the California Institute of Technology with funds from the National Science Foundation, the National Aeronautics and Space Administration, the National Geographic Society, the Sloan Foundation, the Samuel Oschin Foundation, and the Eastman Kodak Cor-

poration. The Oschin Schmidt Telescope is operated by the California Institute of Technology and Palomar Observatory. This paper has made use of NASA’s *SkyView* facility (<http://skyview.gsfc.nasa.gov>) located at NASA Goddard Space Flight Center. NRAO is a facility of the National Science Foundation operated under cooperative agreement by Associated Universities, Inc. B.M.G. acknowledges the support of NASA through Chandra grant GO5-6052X and LTSA grant NAG5-13032. P.O.S. acknowledges support from NASA contract NAS8-39073. F.C. acknowledges the support of the National Science Foundation through grant AST-05-07376.

Facilities: CXO (ACIS), VLA

REFERENCES

- Asaoka, I. & Aschenbach, B. 1994, *A&A*, 284, 573
 Bocchino, F. & Bykov, A. M. 2001, *A&A*, 376, 248
 Bucciantini, N. 2002, *A&A*, 387, 1066
 Bucciantini, N., Amato, E., & Del Zanna, L. 2005, *A&A*, 434, 189
 Burton, M. G., Geballe, T. R., Brand, P. W. J. L., & Webster, A. S. 1988, *MNRAS*, 231, 617
 Caraveo, P. A., Bignami, G. F., DeLuca, A., Mereghetti, S., Pellizzoni, A., Mignani, R., Tur, A., & Becker, W. 2003, *Science*, 301, 1345
 Chevalier, R. A. 1999, *ApJ*, 511, 798
 Chevalier, R. A. 2000, *ApJ*, 539, L45
 Del Zanna, L., Amato, E., & Bucciantini, N. 2004, *A&A*, 421, 1063
 Gaensler, B. M., Arons, J., Kaspi, V. M., Pivovarov, M. J., Kawai, N., & Tamura, K. 2002a, *ApJ*, 569, 878
 Gaensler, B. M., Jones, D. H., & Stappers, B. W. 2002b, *ApJ*, 580, L137
 Gaensler, B. M. & Slane, P. O. 2006, *Ann. Rev. Astr. Ap.*, 44, 17
 Gaensler, B. M., van der Swaluw, E., Camilo, F., Kaspi, V. M., Baganoff, F. K., Yusef-Zadeh, F., & Manchester, R. N. 2004, *ApJ*, 616, 383 (G2004)
 Gvaramadze, V. V. 2002, in *Neutron Stars in Supernova Remnants*, ed. P. O. Slane & B. M. Gaensler (San Francisco: Astronomical Society of the Pacific), 23–26
 Helfand, D. J., Gotthelf, E. V., & Halpern, J. P. 2001, *ApJ*, 556, 380
 Hester, J. J., Mori, K., Burrows, D., Gallagher, J. S., Graham, J. R., Halverson, M., Kader, A., Michel, F. C., & Scowen, P. 2002, *ApJ*, 577, L49
 Hobbs, G., Lorimer, D. R., Lyne, A. G., & Kramer, M. 2005, *MNRAS*, 360, 974
 Hughes, J. P., Slane, P. O., Park, S., Roming, P. W. A., & Burrows, D. N. 2003, *ApJ*, 591, L139
 Jackson, M. S. & Halpern, J. P. 2005, *ApJ*, 633, 1114
 Kaminker, A. D., Yakovlev, D. G., & Gnedin, O. Y. 2002, *A&A*, 383, 1076
 Kaspi, V. M., Roberts, M. S. E., & Harding, A. K. 2006, in *Compact Stellar X-ray Sources*, ed. W. H. G. Lewin & M. van der Klis (Cambridge: CUP), pp. 279–339
 Kawasaki, M., Ozaki, M., Nagase, F., Masai, K., Ishida, M., & Petre, R. 2002, *ApJ*, 572, 897
 Komissarov, S. S. & Lyubarsky, Y. E. 2003, *MNRAS*, 344, L93
 —. 2004, *MNRAS*, 349, 779
 Kramer, M., Bell, J. F., Manchester, R. N., Lyne, A. G., Camilo, F., Stairs, I. H., D’Amico, N., Kaspi, V. M., Hobbs, G., Morris, D. J., Crawford, F., Possenti, A., Joshi, B. C., McLaughlin, M. A., Lorimer, D. R., & Faulkner, A. J. 2003, *MNRAS*, 342, 1299
 Lai, D., Chernoff, D. F., & Cordes, J. M. 2001, *ApJ*, 549, 1111
 Leahy, D. A. 2004, *AJ*, 127, 2277
 McGowan, K. E., Zane, S., Cropper, M., Kennea, J. A., Córdova, F. A., Ho, C., Sasseeen, T., & Vestrand, W. T. 2004, *ApJ*, 600, 343
 Mineo, T., Massaro, E., Cusumano, G., & Becker, W. 2002, *A&A*, 392, 181
 Ng, C.-Y. & Romani, R. W. 2004, *ApJ*, 601, 479
 Olbert, C. M., Clearfield, C. R., Williams, N. E., Keohane, J. W., & Frail, D. A. 2001, *ApJ*, 554, L205 (O2001)
 Page, D., Geppert, U., & Weber, F. 2006, *Nucl. Phys. A*, in press (astro-ph/0508056)
 Pavlov, G. G., Zavlin, V. E., Sanwal, D., Burwitz, V., & Garmire, G. P. 2001, *ApJ*, 552, L129
 Stappers, B. W., Gaensler, B. M., Kaspi, V. M., van der Klis, M., & Lewin, W. H. G. 2003, *Science*, 299, 1372
 van der Swaluw, E., Achterberg, A., Gallant, Y. A., Downes, T. P., & Keppens, R. 2003, *A&A*, 397, 913
 van der Swaluw, E., Downes, T. P., & Keegan, R. 2004, *A&A*, 420, 937
 Vigelius, M., et al. 2006, *MNRAS*, submitted
 Weisskopf, M. C., Hester, J. J., Tennant, A. F., Elsner, R. F., Schulz, N. S., Marshall, H. L., Karovska, M., Nichols, J. S., Swartz, D. A., Kolodziejczak, J. J., & O’Dell, S. L. 2000, *ApJ*, 536, L81
 Weisskopf, M. C. & Hughes, J. P. 2006, in *Astrophysics Update 2*, ed. J. W. Mason (Chichester, UK: Springer-Praxis), in press, astro-ph/0511327
 Welsh, B. Y. & Sallmen, S. 2003, *A&A*, 408, 545

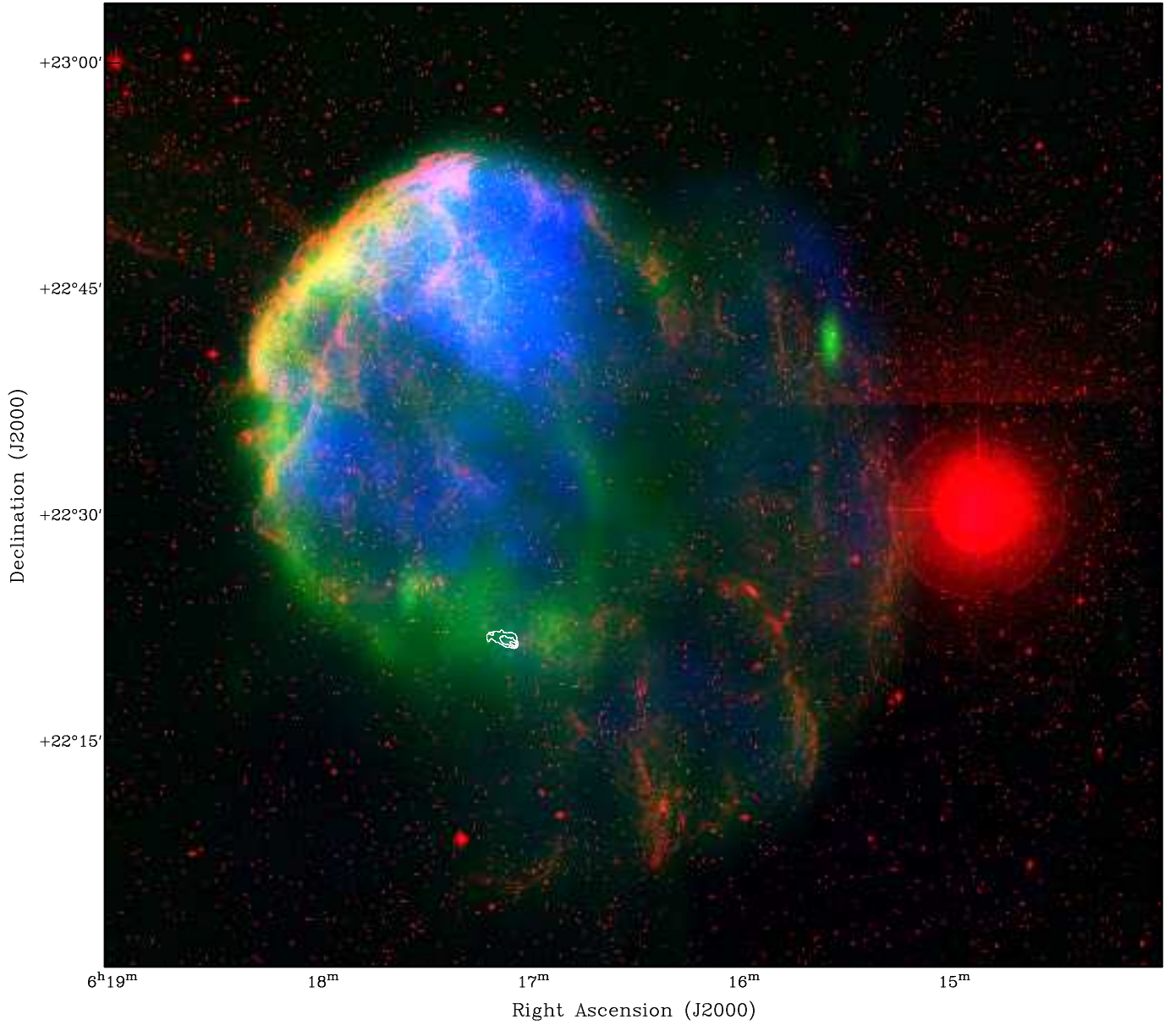


FIG. 1.— A multiwavelength view of the SNR IC 443 and the PWN G189.22+2.90. Red shows 670-nm emission from the Second Palomar Observatory Sky Survey; green shows 1.4-GHz radio data taken by the DRAO Synthesis Telescope (Leahy 2004); blue shows 0.1–2.4 keV X-ray data taken by the *ROSAT* PSPC (Asaoka & Aschenbach 1994). The white contours show 8.5-GHz Very Large Array data on G189.22+2.90 at a resolution of $9'' \times 8''$ (O2001), with contour levels drawn at 20%, 50% and 80% of the peak of $3.7 \text{ mJy beam}^{-1}$. The bright star to the west of IC 443 is η Gem.

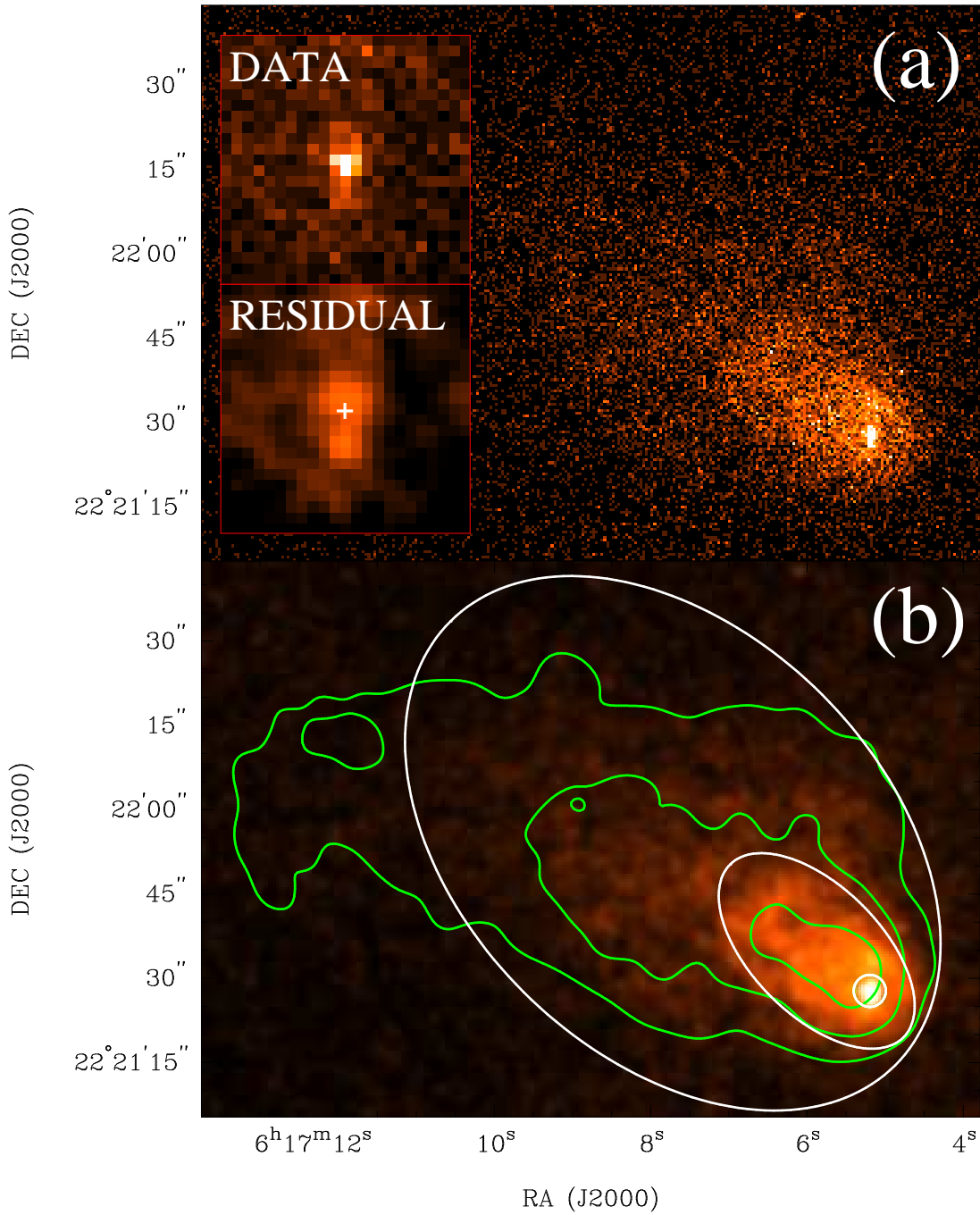


FIG. 2.— X-ray images of the bow shock PWN G189.22+2.90 in SNR IC 443. (a) A *Chandra* image in the energy range 0.3–10 keV, made using the 2005 data and displayed using a linear transfer function ranging from 0 to 9 counts per pixel (the peak value is 85 counts). The insets show the data and the residual after fitting a central gaussian to a $11'' \times 11''$ region surrounding the central source CXOU J061705.3+222127, both on linear scales ranging from 0 to 40 counts per $0''.49 \times 0''.49$ pixel. The residual image has been smoothed with a gaussian of FWHM $1''$ to make clear the existence of faint extended structure on either side of CXOU J061705.3+222127 (the position of CXOU J061705.3+222127 is marked with a white cross). (b) The same data as in panel (a), but smoothed with a gaussian of FWHM $2''$. From the inside out, the white ellipses show the extraction regions for CXOU J061705.3+222127 (for clarity, drawn with a radius twice that actually used), the tongue, and the tail; each region excludes the ones inside it. The green contours show the radio nebula, using the same levels as shown in Fig. 1.

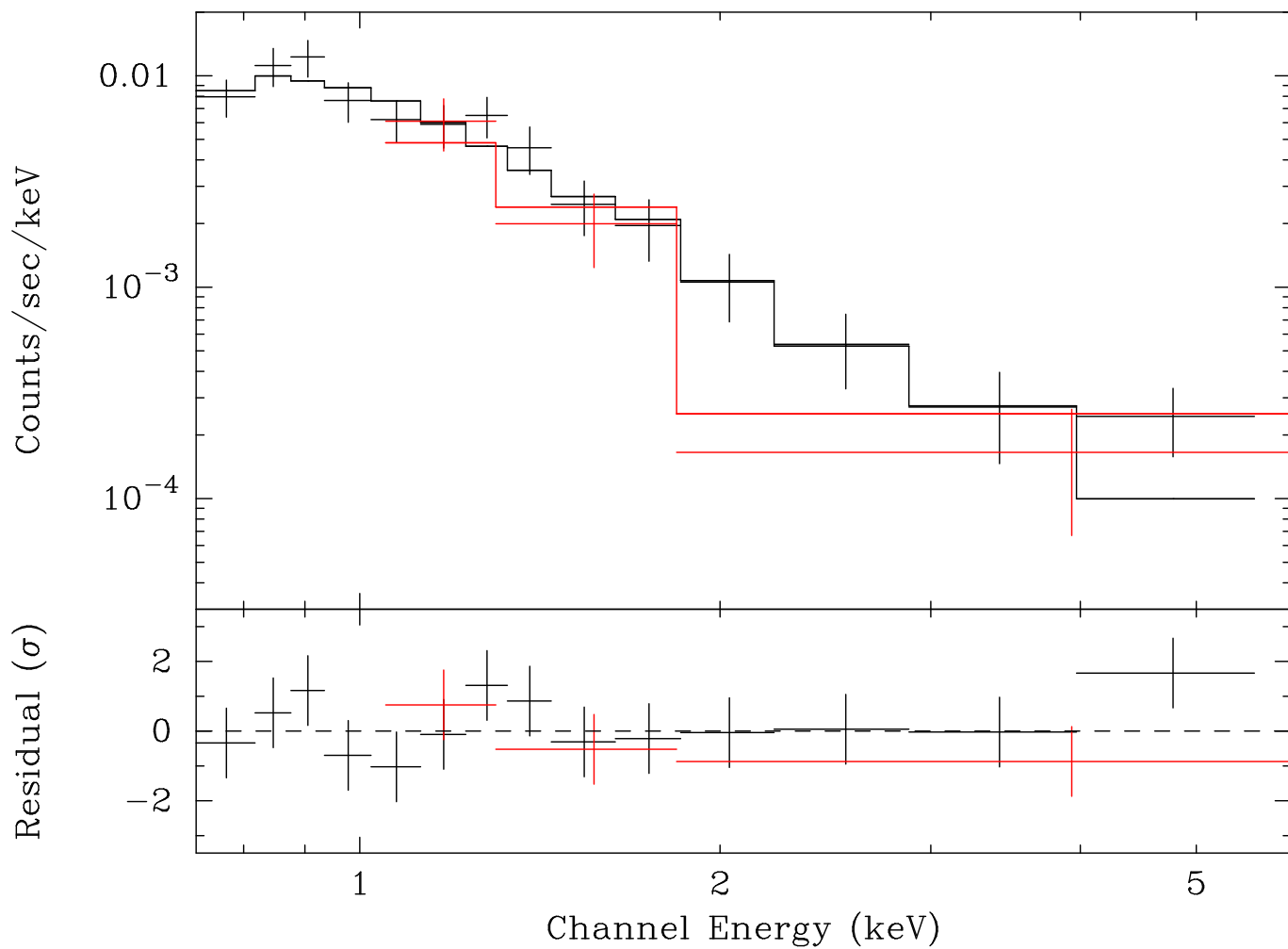


FIG. 3.— *Chandra* ACIS spectra of J0617+2221. The points in the upper panel indicate the data from 2000 (red) and 2005 (black), while the solid lines show the corresponding best fit absorbed blackbody plus power-law models. The lower panel shows the number of standard deviations by which the model and the data differ in each bin.